

# Small $x$ Behavior of Parton Distributions from the Observed Froissart Energy Dependence of the Deep Inelastic Scattering Cross Sections

M. M. Block,<sup>1</sup> Edmond L. Berger,<sup>2</sup> and Chung-I Tan<sup>3</sup>

<sup>1</sup>*Department of Physics and Astronomy,*

*Northwestern University, Evanston, IL 60208*

<sup>2</sup>*High Energy Physics Division, Argonne National Laboratory, Argonne, Illinois 60439*

<sup>3</sup>*Physics Department, Brown University, Providence, RI 02912*

(Dated: August 8, 2018)

## Abstract

We fit the reduced cross section for deep-inelastic electron scattering data to a three parameter  $\ln^2 s$  fit,  $A + \beta \ln^2(s/s_0)$ , where  $s = \frac{Q^2}{x}(1-x) + m^2$ , and  $Q^2$  is the virtuality of the exchanged photon. Over a wide range in  $Q^2$  ( $0.11 \leq Q^2 \leq 1200 \text{ GeV}^2$ ) all of the fits satisfy the logarithmic energy dependence of the Froissart bound. We can use these results to extrapolate to very large energies and hence to very small values of Bjorken  $x$  — well beyond the range accessible experimentally. As  $Q^2 \rightarrow \infty$ , the structure function  $F_2^p(x, Q^2)$  exhibits Bjorken scaling, within experimental errors. We obtain new constraints on the behavior of quark and antiquark distribution functions at small  $x$ .

PACS numbers: 13.60.Hb, 12.38.-t, 12.38.Qk

*Introduction.* Inclusive deep-inelastic lepton scattering (DIS) has played a seminal role in particle and nuclear physics, notably for its early manifestation of Bjorken scaling [1] and, soon thereafter, the logarithmic scaling violations that are a hallmark of perturbative quantum chromodynamics. From the structure functions of DIS, one also obtains crucial constraints on the parton distribution functions essential for predictions of short-distance hard-scattering phenomena at very high energies, whether at hadron collider facilities or in ultra high energy cosmic ray interactions. The DIS lepton-nucleon cross sections may also be analyzed in complementary fashion as hadronic  $Vp$  scattering cross sections, where  $V = \gamma^*$ , a virtual photon in the case of electron-nucleon scattering. We show explicitly in this Letter that the reduced  $\gamma^*p$  total cross sections manifest the Froissart  $\ln^2 s$  growth [2] with hadronic energy  $s$  that also characterizes the  $\gamma p$ ,  $\pi^\pm p$  and  $\bar{p}p$  and  $pp$  cross sections at very high energy [3]. Our fits to 28 different  $Q^2$  data sets of  $F_2^p(x, Q^2)$  demonstrate that a  $\ln^2 s$  growth holds for each of the virtual photon's mass  $Q^2$ . This observation allows us to obtain a new constraint on the Bjorken  $x$  dependence of the quark and antiquark parton distribution functions at small  $x$ , viz., they should behave at very small  $x$  as  $\beta \log^2(x_0/x)$ , for all  $Q^2 \gg m^2$ , where  $m$  is the proton mass, and  $\beta$  and  $x_0$  are functions of  $Q^2$ . As  $x \rightarrow 0$  and  $Q^2 \rightarrow \infty$ ,  $\beta$  and  $x_0$  approach constant values  $\beta'$ ,  $x'_0$ . Only 6 parameters are needed to fit 28 data sets, allowing us in principle to extrapolate to very large energies and very low  $x$ , well beyond the experimental range presently accessible, with confidence that we understand the  $x$  dependence of structure functions and parton distribution functions for “wee” partons.

*Kinematics.* In the inclusive process  $ep \rightarrow e'X$ , the laboratory four-vector momentum of the exchanged virtual photon  $\gamma^*$  is  $q = (\nu, \vec{q})$ , with negative  $q^2 \equiv -Q^2$ , and the proton laboratory four-vector momentum is  $p = (m, 0)$ . The invariant  $s$ , the square of the center of mass (c.m.) energy  $W$  of the  $\gamma^*p$  system, is  $s \equiv W^2 = (q + p)^2 = 2m\nu - Q^2 + m^2$ . The Lorentz invariant variables  $x$  and  $y$  are defined as  $x \equiv \frac{Q^2}{2p \cdot q} = \frac{Q^2}{2m\nu}$  and  $y \equiv \frac{p \cdot q}{p \cdot k}$ , where  $k$  is the incoming electron's four-vector momentum. Thus,

$$s = W^2 = \frac{Q^2}{x}(1 - x) + m^2. \quad (1)$$

In terms of  $x$ ,  $y$  and  $Q^2$ , the cross section for  $ep \rightarrow e'X$  may be expressed as

$$\begin{aligned} \frac{d^2\sigma(x, y, Q^2)}{dx dQ^2} &= \frac{2\pi\alpha^2}{Q^4 x} \left( 2 - 2y + \frac{y^2}{1 + R} \right) F_2^p(x, Q^2) \\ &\equiv \Gamma \times \sigma_{\gamma^*p}^{\text{eff}}(x, y, Q^2). \end{aligned} \quad (2)$$

Here,  $F_2^p(x, Q^2)$  is the dimensionless proton structure function,  $R \equiv \frac{F_L}{F_2 - F_L}$ , with  $F_L$  being the longitudinal structure function,  $\alpha$  the fine structure constant, and  $\Gamma \equiv \alpha(2 - 2y + y^2)/(2\pi Q^2 x)$ .

The quantity measured experimentally,  $\sigma_{\gamma^*p}^{\text{eff}}(x, y, Q^2)$ , is a function of 3 variables,  $x, y$  and  $Q^2$ . We define the total virtual photon cross section  $\sigma_{\gamma^*p}^{\text{tot}}(x, Q^2)$ , a function of only two variables,  $x$  and  $Q^2$ , as

$$\sigma_{\gamma^*p}^{\text{tot}} \equiv \sigma_{\text{T}}(x, Q^2) + \sigma_{\text{L}}(x, Q^2) \quad (3)$$

$$= \frac{4\pi^2\alpha}{Q^2} \times \left( \frac{1 + 4m^2x^2/Q^2}{1 - x} \right) F_2^p(x, Q^2) \quad (4)$$

$$\approx \frac{4\pi^2\alpha}{Q^2} \times \frac{F_2^p(x, Q^2)}{1 - x}, \quad Q^2 \gg 4m^2x^2. \quad (5)$$

In Eq. (3),  $\sigma_{\text{T}}(x, Q^2)$  and  $\sigma_{\text{L}}(x, Q^2)$  denote the transverse and longitudinal virtual photon cross sections.

*Saturation of the Froissart bound.* High energy cross sections for hadron-hadron scattering must be bounded by  $\sigma \sim \ln^2 s$ , where  $s$  is the square of the c.m. energy. This fundamental result is derived from unitarity and analyticity by Froissart [2]. Saturation of the Froissart bound refers to an energy dependence of the total cross section rising no more rapidly than  $\ln^2 s$ .

It has been shown that the Froissart bound is *saturated* at high energies [3] in  $\gamma p$ ,  $\pi^\pm p$  and  $\bar{p}p$  and  $pp$  scattering, and, as we now will show, also in  $\gamma^*p$  scattering.

We choose to work in terms of a dimensionless “reduced”  $\gamma^*p$  cross section,  $\sigma_{\gamma^*p}^{\text{tot}}(W, Q^2)/\kappa$ , where  $\kappa \equiv 4\pi^2\alpha/Q^2$ . Using the parameterization of Block and Cahn [4], we write the reduced cross section<sup>1</sup> as

$$\sigma_{\gamma^*p}^{\text{tot}}(W, Q^2)/\kappa = A + \beta \ln^2 \frac{s}{s_0} + cs^{-0.5}. \quad (6)$$

The 4 coefficients  $A, \beta, s_0$ , and  $c$  are functions of  $Q^2$ . We present fits to 29 data sets published by the ZEUS [5] collaboration<sup>2</sup>, for  $Q^2 = 0.11, 0.20, 0.25, 0.65, 2.7, 3.5, 4.5, 6.5, 8.5, 10, 12, 15, 18, 22, 27, 35, 45, 60, 70, 90, 120, 150, 200, 250, 350, 450, 650, 800$ , and

<sup>1</sup> The parameterization of Eq. (6) is the same as that used by Block and Halzen [3] for their successful fits of hadronic cross sections for  $\gamma p$ ,  $\pi^\pm p$  and  $\bar{p}p$  and  $pp$  scattering, except for a transformation of variables.

<sup>2</sup> In order to avoid possible normalization differences, we have not included H1 data [6] in our analysis, although preliminary examination of the combined data sets leads us to identical physics conclusions.

1200 GeV<sup>2</sup>. Prior to displaying and discussing our fits, we make three observations about the data:

- An examination of plots of  $F_2^p(x, Q^2)$  versus  $x$  for different values of  $Q^2$  shows that all data sets are compatible with going through a *common* point at  $x \approx 0.09$  and  $F_2 \approx 0.41$ . We call this common intersection the “scaling” point  $x_P$  and examine its significance below.
- Inspection of  $F_2^p(x, Q^2)$  versus  $x$  shows that for  $x \leq x_P$  and  $Q^2 \gtrsim 350$  GeV<sup>2</sup>, the data overlap each other, i.e., within experimental uncertainties, they scale in Bjorken  $x$  (see footnote 4).
- When plotted as  $\sigma_{\gamma^*p}^{\text{tot}}/\kappa$  versus  $W$ , with a logarithmic  $W$  axis, the data at all  $Q^2$  show similar parabolic shapes for  $x \leq x_P$ , rising with  $W$ , with the shape parameters depending slowly on  $Q^2$ , with a negligible inverse-power term proportional to  $c$ .

Introducing  $x$  from Eq. (1), defining the parameter  $x_0(Q^2) \equiv Q^2/s_0$ , and setting  $c = 0$ , we find that Eq. (6) becomes, for  $x \leq x_P$ ,

$$\sigma_{\gamma^*p}^{\text{tot}}(x, Q^2)/\kappa = A + \beta \ln^2 \left[ x_0 \frac{1-x}{x} + \frac{x_0 m^2}{Q^2} \right]. \quad (7)$$

For  $Q^2 \gg m^2$  and  $x \leq x_P$ , we obtain the closed forms

$$\sigma_{\gamma^*p}^{\text{tot}}(x, Q^2)/\kappa = A + \beta \ln^2 \left[ x_0 \frac{1-x}{x} \right], \quad (8)$$

$$F_2^p(x, Q^2) = (1-x) \left( A + \beta \ln^2 \left[ x_0 \frac{1-x}{x} \right] \right), \quad (9)$$

where  $A$ ,  $\beta$ , and  $x_0$  are functions of  $Q^2$ .

In order to bolster the above observations quantitatively, we made  $\chi^2$  fits of Eq. (7) to 29 sets of the Zeus data, i.e., using the  $\ln^2 s$  parameterization of Eq. (6) with  $c = 0$ , with the added requirement that each curve go through its appropriate  $(W_P(Q^2), \sigma_{\gamma^*p}^{\text{tot}}(W_P, Q^2)/\kappa)$  scaling point, where

$$W_P(Q^2) \equiv W(Q^2, x_P) = \sqrt{\frac{Q^2}{x_P}(1-x_P) + m^2}. \quad (10)$$

We fit only those data with  $x \leq x_P$ , corresponding to  $W > W_P$ , which is our definition of high energy data. We treat the 5 highest  $Q^2$  data sets,  $Q^2 = 350, 450, 650$ ,

800 and 1200 GeV<sup>2</sup>, as one set, since their  $F_2^p(x)$  data points overlap. From fits to individual sets of points with common  $Q^2$ , we find that over the range<sup>3</sup>  $0.11 \leq Q^2 \leq 1200$  GeV<sup>2</sup>, and for energies  $W \geq W_P$ , each data set with a common  $Q^2$  is fit satisfactorily with the 3 parameters  $A, \beta$  and  $s_0$ , with  $A$  constrained by

$$A = \sigma_{\gamma^*p}^{\text{tot}}(W_P, Q^2)/\kappa - \beta \ln^2 \frac{W_P^2}{s_0}. \quad (11)$$

Our results are illustrated in Fig. 1, where we plot the reduced cross section vs. the c.m. energy  $W$  for the Zeus [5] high energy data, together with our constrained fits. We use their published values of  $F_2^p(x)$  and for errors, their statistical and systematic errors taken in quadrature. All of the data<sup>4</sup> agree well with a  $\ln^2 s$  parameterization over this wide  $Q^2$  range. Also shown in Fig. 1 as large bold points are the 11 different values of  $W(x_P)$  that correspond to the scaling point  $x_P = 0.09$ ,  $F_2^p(x_P) = 0.41$ .

The agreement with experiment, over the broad range of  $Q^2$  investigated here, is seen perhaps more clearly in the plot of  $F_2^p(x)$  vs.  $x$ , shown in Fig. 2. This figure shows the same  $Q^2$  sets as in Fig. 1, along with the same 11 constrained  $\ln^2 s$  fits of the form specified in Eq. (7), with  $A$  constrained by Eq. (11). Careful examination of Fig. 2 shows that the data are in excellent agreement with the hypothesis that all of the widely different  $Q^2$  fits intersect at the point  $x_P = 0.09$ ,  $F_2^p(x_P) = 0.41$ , i.e., it's is a very good scaling point, being satisfied by all of the ZEUS [5] sets as well as the BCDMS collaboration points [7].

Having a scaling point gives us a universal anchor point—an *analyticity constraint* [8]—for the fits to the different sets of values of  $Q^2$ . As shown in Eq. (11), only 2 parameters,  $\beta$  and  $x_0 \equiv Q^2/s_0$ , are now required for the fit to each  $Q^2$  data set. This reduction in the number of parameters constrains their values, making the fit uncertainties considerably smaller, e.g., the fractional error in  $F_2^p$  due to parameter uncertainties is  $\sim 5\%$ , for both  $x = 10^{-6}$ ,  $Q^2 = 3.5$  GeV<sup>2</sup> and  $x = 10^{-3}$ ,  $Q^2 = 1200$  GeV<sup>2</sup>.

Although not shown explicitly here, we find that the coefficients  $\beta$  and  $x_0$  are smoothly

---

<sup>3</sup> For  $Q^2 > 1200$  GeV<sup>2</sup>, there are essentially no ZEUS data with  $W > W_P(1200 \text{ GeV}^2)$ , so we stop our fits at  $Q^2 = 1200$  GeV<sup>2</sup>.

<sup>4</sup> Although not shown in Fig. 1 to avoid loss of clarity, we have also made constrained fits for  $Q^2 = 2.7, 4.5, 8.5, 12, 15, 18, 27, 35, 45, 60, 120, 150, 200$  and  $250$  GeV<sup>2</sup>, with similar results, a total of 25 fits to independent data sets at different  $Q^2$ . We found a total  $\chi^2 = 113.56$  for 164 degrees of freedom, corresponding to  $\chi^2/d.f. = 0.692$ . For the 5 combined data sets at the highest  $Q^2$ , we found  $\chi^2 = 26.99$  for 27 degrees of freedom, *a posteriori* justifying our combining them into a single set labeled 1200.

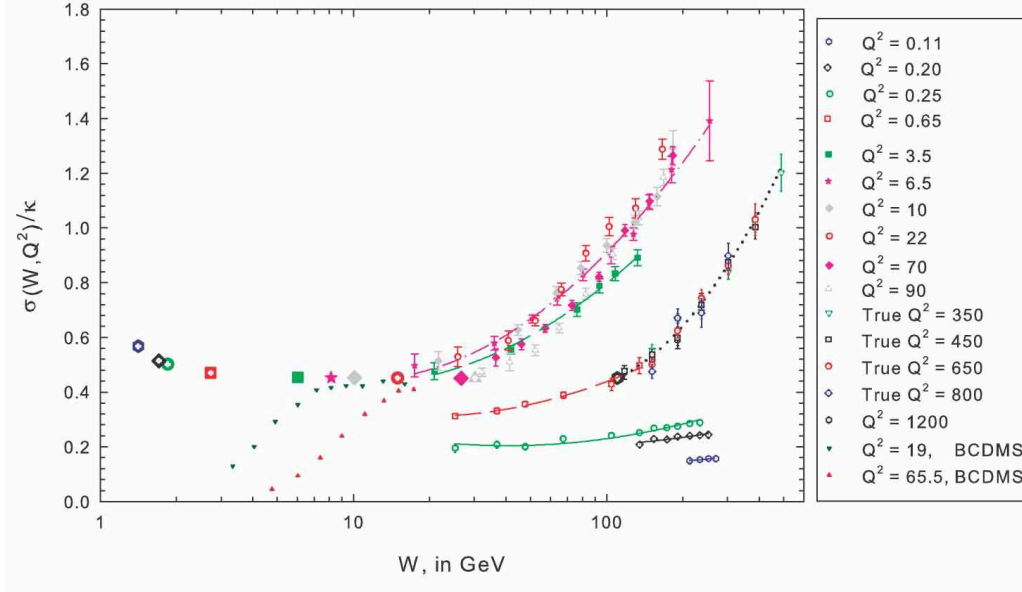


FIG. 1: The reduced cross section  $\sigma_{\gamma^*p}^{\text{tot}}(W, Q^2)/\kappa$  vs.  $W$ , in GeV, with  $\kappa = 4\pi^2\alpha/Q^2$ . The high energy Zeus [5] data plotted here have  $x \leq x_P$ . The curves are  $\ln^2 s$  fits,  $\sigma_{\gamma^*p}^{\text{tot}}/\kappa = A + \beta \ln^2(W^2/s_0)$ , forced to go through the scaling point  $x_P, F_2^p(x_P)$ . The 11 *large* symbols,  $W_P(Q^2)$ , correspond to the common intersection (scaling) point shown in Fig. 2. The very tiny points, data from the BCDMS collaboration [7], are not used in the fits. The data labeled “true  $Q^2 =$ ” are fit as if they had been part of the  $Q^2 = 1200 \text{ GeV}^2$  set.

varying functions of  $Q^2$ , both being parameterized adequately as

$$\ln x_0 = \ln x'_0 + \frac{a_1}{(Q^2)^{a_2}}, \quad (12)$$

$$\beta = \beta' - \frac{b_1}{(Q^2)^{b_2}}, \quad (13)$$

where the constants  $\beta'$  and  $x'_0$  are given by

$$\beta', x'_0 = \lim_{Q^2 \rightarrow \infty} \beta(Q^2), x_0(Q^2). \quad (14)$$

The 6 constants  $\beta', x'_0, a_1, a_2, b_1$  and  $b_2$  are parameters that can be obtained in a global fit. In a truly global fit, in addition to these 6 constants we need the two scaling point coordinates  $x_P, F_2^p(x_P)$ , i.e., a total of 8 parameters, in order to fit all the available data on  $F_2^p(x, Q^2)$ . This Letter demonstrates the feasibility of such a fit.

Attention may be drawn to the fits for  $Q^2 = 0.11, 0.20, 0.25$  and  $0.65 \text{ GeV}^2$  in Figs. 1 and 2. These curves do not show different shapes in  $W - \sigma/\kappa$  space from any of their counterparts

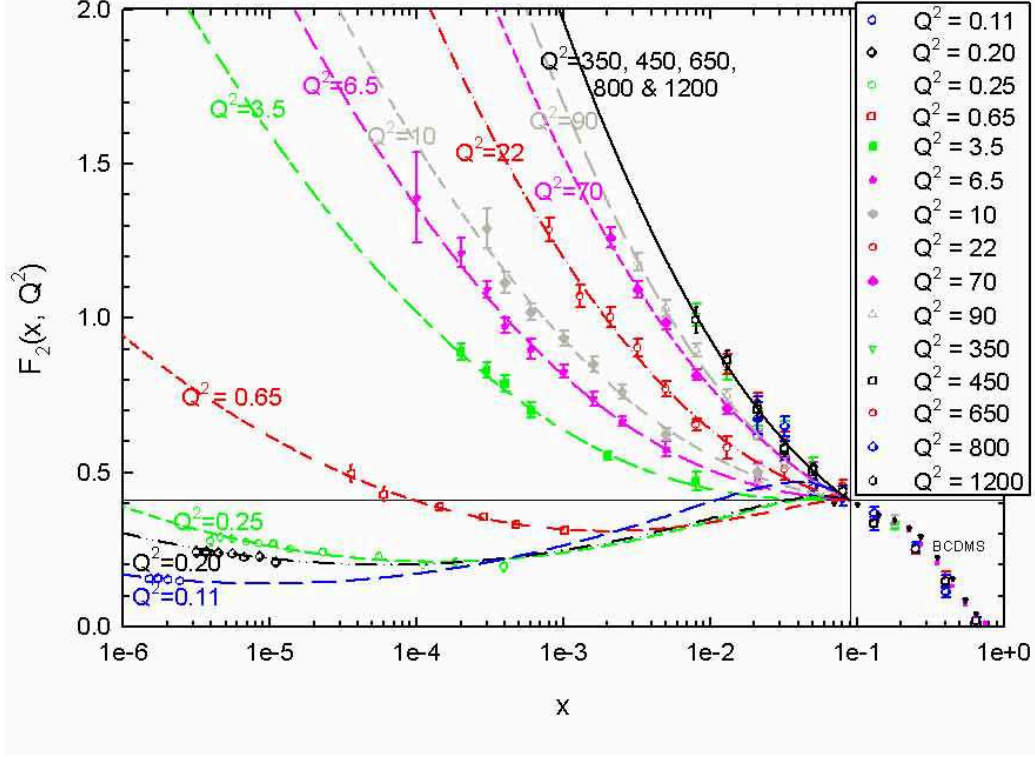


FIG. 2: Fits to the proton structure function data,  $F_2^p(x, Q^2)$  vs.  $x$ , for 15 values of  $Q^2$ . The data are those of Fig. 1. The curves are the  $\ln^2 s$  fits of Fig. 1, converted to the  $F_2^p - x$  plane. The tiny points are BCDMS [7] data. The vertical and horizontal straight lines intersect at the scaling point  $x_P = 0.09, F_2^p(x_P) = 0.41$ . The data for  $Q^2 = 350, 450, 650, 800$  and  $1200 \text{ GeV}^2$  are all fit together with a single curve.

at larger  $Q^2$ —since they also are parabolic in shape—but they exhibit more structure than the other curves when plotted in  $F_2^p - x$  space. This shape difference is explained by their very low values of  $Q^2$ . The term  $1 + 4m^2x^2/Q^2$  in Eq. (4) becomes substantially greater than unity as  $x \rightarrow x_P$ , and in the relation  $\frac{Q^2}{x}(1-x) = W^2 - m^2$  of Eq. (1),  $\frac{Q^2}{x}(1-x) \approx 2m(W-m)$  for small  $Q^2$  and  $x \lesssim x_P$ ; these terms strongly influence the transformation from  $\sigma_{\gamma^*p}^{\text{tot}}/\kappa - W$  space to  $F_2^p - x$  space when  $Q^2$  is very small. We find that one closed form fits *all* of the  $Q^2$  data for  $x \leq x_P$ , i.e.,

$$F_2^p(x, Q^2) = \frac{1-x}{1+4m^2x^2/Q^2} \times \left\{ A + \beta \ln^2 \left[ x_0 \frac{1-x}{x} \left( 1 + \frac{m^2}{Q^2} \frac{x}{1-x} \right) \right] \right\}. \quad (15)$$

*Implications for parton distribution functions.* The structure function  $F_2^p(x, Q^2)$  has a simple interpretation in the parton model in which the scattering from the proton is due entirely to the scattering from its individual constituents. Only the quarks and antiquarks couple directly to the electroweak current carried by the virtual photon  $\gamma^*$  in DIS. The DIS cross section may then be expressed in terms of the probabilities  $q_{f/h}(x)$  of finding a quark, and  $\bar{q}_{f/h}(x)$  of finding an antiquark, of flavor  $f$  and fractional momentum  $x$  in hadron  $h$ , times the cross section for the elastic scattering of that parton. As a consequence of gluon radiation in quantum chromodynamics (QCD), the quark, antiquark, and gluon densities become functions of  $Q^2$  as well as  $x$ , e.g.,  $q_{f/h}(x) \rightarrow q_{f/h}(x, Q^2)$ .

The precise expression for  $F_2(x, Q^2)$  in terms of parton distributions depends on the choice of the factorization scheme in QCD. The most commonly used schemes are the DIS and the modified minimal subtraction  $\overline{\text{MS}}$  schemes. In the DIS scheme, all higher-order contributions to the structure functions  $F_2(x, Q^2)$  are absorbed into the distributions of the quarks and antiquarks [9], and we may write, to all orders in QCD,

$$F_2(x, Q^2) = \sum_f e_f^2 x (q_{f/h}^{\text{DIS}}(x, Q^2) + \bar{q}_{f/h}^{\text{DIS}}(x, Q^2)), \quad (16)$$

where  $e_f$  is the fractional electric charge of flavor  $f$ . The superscripts DIS indicate that the distributions are those defined in the DIS scheme. In QCD, gluon radiation removes momentum at large  $x$ , decreasing the value of  $F_2^p(x, Q^2)$  as  $Q^2$  grows, and builds up the quark and antiquark distributions at small  $x$ , leading to the qualitative expectation of the *scaling* point that we observe in  $x$  at which  $F_2^p(x_P, Q^2)$  is independent of  $Q^2$ .

The Froissart  $\ln^2(s/s_0)$  energy dependence of the data allows us to conclude, for  $x \leq x_P$  and  $Q^2 \gg m^2$ , that

$$xq_{f/h}^{\text{DIS}}(x, Q^2) \sim (1-x) \times \left( A + \beta \ln^2 \left[ x_0 \frac{1-x}{x} \right] \right). \quad (17)$$

Moreover, within experimental errors, we find that

$$\begin{aligned} xq_{f/h}^{\text{DIS}}(x, Q^2 \gtrsim 350 \text{ GeV}^2) &\approx xq_{f/h}^{\text{DIS}}(x) \\ &\sim (1-x) \times \left( A' + \beta' \ln^2 \left[ x'_0 \frac{1-x}{x} \right] \right), \end{aligned} \quad (18)$$

with  $Q^2$ -independent values  $A' = 0.40$ ,  $\beta' = 0.050 \pm 0.008$ , and  $x'_0 = 0.28 \pm 0.01$ .

Parton distribution functions of quarks, antiquarks, and gluons are generally extracted from a global fit [11] to a wide class of hard scattering data including deep-inelastic scattering cross sections. Typically one begins with assumed parameterizations of the  $x$  dependence



of the distributions at a fixed low value  $Q_0$  and then uses the perturbative evolution equations [10] of QCD to obtain the  $x$  and  $Q^2$  dependences of these distributions for all  $Q > Q_0$ . The non-perturbative form that is assumed in the CTEQ parameterization, for example, for these distributions has power behavior at small  $x$ ,  $xf(x, Q_0) \sim x^A$ . We contrast this power behavior with the logarithmic behavior that is shown by the data, suggesting that it is productive to redo a global fit program using logarithmic behavior at small  $x$ . Over a small range of  $x$  one cannot distinguish a logarithmic and a power expression with small fractional power (e.g.,  $\sim 0.25$ ), but the behavior of these expressions is clearly different when extrapolated over a very great range.

In conclusion, we demonstrated that we can make simultaneous  $\ln^2 s$  fits saturating the Froissart bound, to 218 ZEUS datum points, with all fits going through the same scaling point, strongly constraining the behavior of  $F_2^p(x, Q^2)$  at tiny  $x$ . These fits are made with only 2 parameters per set of data with common  $Q^2$ , since the analyticity constraint [8] of Eq. (11) on the cross section at the scaling point requires only the 2 coefficients,  $\beta(Q^2)$ ,  $x_0(Q^2)$ . This additional constraint insures a well determined set of fit parameters, and thus an accurate forecast of the very small  $x$  behavior. Saturation of the Froissart bound allows us to project to very large  $W$  and hence to very small  $x$  with a high degree of confidence in our functional form. Our demonstration of Froissart energy dependence at small  $x$  for each  $Q^2$  should shed light on various theoretical efforts in examining small  $x$  physics in QCD and on parton saturation at high density [12]. Our program for the future includes a global constrained  $\ln^2 s$  fit, as described above, to all available  $F_2^p$  data, in order to obtain the necessary parameters and their uncertainties needed to extract accurate parton distribution functions at small  $x$ .

E.L.B. is supported by the U. S. Department of Energy, Division of High Energy Physics, under Contract No. W-31-109-ENG-38. C-I.T. is supported in part by the U. S. Department of Energy under Contract DE-FG02-91ER40688, TASK A. E.L.B. and M.M.B. thank the Aspen Center for Physics for its hospitality during the writing of this paper. E.L.B. thanks Professor Jianwei Qiu for valuable comments, and M.M.B. thanks Professors L. Durand III, S. Gasiorowicz, and F. Halzen for providing new insights and most valuable discussions.

- 
- [1] J. D. Bjorken, Phys. Rev **179**, 1547 (1969); J. I. Friedman and H. W. Kendall, Ann. Rev. Nucl. Part. Sci. **22**, 203 (1972).
- [2] M. Froissart, Phys. Rev. **123**, 1053 (1961).
- [3] M. M. Block and F. Halzen, Phys. Rev D **70**, 091901 (2004); M. M. Block and F. Halzen, Phys. Rev D **72**, 036006 (2005).
- [4] M. M. Block and R. N. Cahn, Rev. Mod. Phys. **57**, 563 (1985).
- [5] ZEUS Collaboration, V. Chekanov et al, Eur. Phys. J. **21**, 443 (2001).
- [6] H1 collaboration, E. Adloff et al., Eur. Phys. J. **C13**, 609 (2000); Eur. Phys. J. **C21**, 33 (2001).
- [7] BCDMS Collaboration, A. C. Benvenuti et al., Phys. Lett. **B233**, 465 (1989).
- [8] M. M. Block, Eur. Phys. J. **C47**, 697 (2006).
- [9] G. Altarelli, R. K. Ellis, and G. Martinelli, Nucl. Phys. **B157**, 461 (1979).
- [10] V. N. Gribov and L. N. Lipatov, Sov. J. Nucl. Phys. **15**, 438 (1972); G. Altarelli and G. Parisi, Nucl. Phys. **B126**, 298 (1977).
- [11] CTEQ Collaboration, J. Pumplin *et al*, JHEP **0207**, 012 (2002); MRTS Collaboration, A. D. Martin, et al., Eur. Phys. J. **C35** 325 (2004).
- [12] L. N. Lipatov, Phys. Rept. **286**, 131 (1997); A. H. Mueller, Nucl. Phys. **B437**, 107 (1995); D. Kharzeev, E. Levin, and L. McLerran, Phys. Lett. **B561**, 93 (2003).